Acidity Differences between Inorganic Solids Induced by Their Framework Structure. A Combined Quantum Mechanics/Molecular Mechanics ab Initio Study on Zeolites

Martin Brändle[†] and Joachim Sauer*

Contribution from Humboldt-Universität zu Berlin, Institut für Chemie, Arbeitsgruppe Quantenchemie, Jägerstr. 10/11, D-10117 Berlin, Germany

Received August 18, 1997

Abstract: The influence of the zeolite framework type (FAU, CHA, MOR, MFI) and the crystallographic position on the acidity of zeolites is investigated. The most stable Brønsted acid sites of the high-silica frameworks are considered: O1−H (FAU), O1−H (CHA), Al4−O2(H)−Si (MOR), and Al7−O17(H)−Si4 (MFI, sinusoidal channel). The latter is compared with the less stable Al12-O24(H)-Si12 position (MFI, channel intersection). Both the heat of the deprotonation and the heat of ammonia adsorption are considered as measures of acid strength. A novel hybrid computational scheme is used that combines the quantum mechanical cluster description (QM) of the active site with interatomic potentials (Pot) for the periodic zeolite framework. Specifically, the Hartree−Fock method (QM) is combined with ab initio shell model potentials (Pot) for the zeolite framework and its interaction with ammonia and ammonium ions. Complete relaxation of the framework is possible within this scheme and long-range corrections to the reaction energies are obtained from the shell model potentials. The total QM-Pot reaction energies are remarkably stable with increasing cluster size. The calculated heats of deprotonation suggest the acidity sequence Y (1171 kJ/mol) > CHA (1190 kJ/mol) > MOR (1195 kJ/mol) > ZSM-5 (1200 kJ/mol), which is neither explained by local structure effects nor by crystal potential effects alone. The calculated heats of NH_3 adsorption suggest the sequence MOR > CHA ≈ Y > ZSM-5. The different order is caused by specific interactions of NH_4^+ with the negatively charged catalyst surface. The predicted heats of NH_3 adsorption are −119, −114, −113, and −109 kJ/mol, respectively. Comparison is made with microcalorimetry and TPD data.

1. Introduction

For gas-phase molecules, Brønsted acidity is well-understood[1] and theoretical predictions can be made with an accuracy that matches that of experiments.[2,3] The understanding of Brønsted acidity of inorganic solids is much less advanced, in spite of the important role that these materials play as catalysts in industrial processes and the enormous amount of research that has been made and is being made. Major research goals have been to find reliable experimental techniques for characterizing the acid strength of different sites in different catalysts and to understand the observed changes of the acidity when varying the structure of the catalysts and their composition. Protonated zeolites are particularly useful catalysts.[4,5] Over the last 10 years about 3400 papers have been published dealing with these materials only. Their microporous structure provides a large internal surface and adds shape-selectivity to their function. The active sites are the bridging hydroxyl groups.

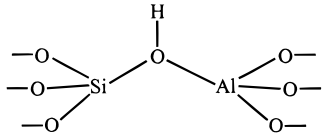

The catalytic activity can be characterized by the *n*-hexane cracking rate. A linear increase of the activity with the Al content in the framework was found,[6] as long as the sites could be considered as noninteracting. We are interested in the acid strength of such isolated sites, specifically in the differences in acid strength between Brønsted sites in different frameworks, i.e., faujasite, chabazite, mordenite, and ZSM-5.

For gas-phase molecules there is a well-established acidity scale. Acidity is clearly defined as enthalpy of deprotonation. Such data are available from measuring proton-transfer equilibria in mass or pulsed ion cyclotron resonance spectrometers and entropy estimates.[1] To surface hydroxyl groups these types of techniques are not applicable. Instead, inferences have been made from frequency shifts of the OH infrared (IR) band on adsorption of proton acceptor molecules. Deprotonation enthalpies are estimated by comparing the frequency shifts observed for OH acids in the gas phase with those of surface hydroxyls using the same set of base molecules (Bellamy−

* Corresponding author.
[†] Present address: ETH Zürich, Laboratorium für anorganische Chemie, Universitätstr. 6, CH-8092 Zürich, Switzerland.

(1) Bartmess, J. E.; McIver, R. T., Jr. In *Gas Phase Ion Chemistry*; Bowers, M. T., Ed.; Academic Press: New York, 1979; p 87, Vol. 2.
(2) Curtiss, L. A.; Raghavachari, K.; Trucks, G. W.; Pople, J. A. *J. Chem. Phys.* **1991**, *94*, 7221.
(3) Sauer, J.; Ahlrichs, R. *J. Chem. Phys.* **1990**, *93*, 2575.
(4) Sie, S. T. In *Advanced Zeolite Science and Applications*; Jansen, J. C., Stöcker, M., Karge, H. G., Weitkamp, J., Eds. *Stud. Surf. Sci. Catal.* **1994**, *85*, 587.
(5) (a) Meisel, S. L.; McCullough, J. P.; Lechthaler, C. H.; Weisz, P. B. *CHEMTECH* **1976**, *6*, 86. (b) Gabelica, Z. In *Zeolites: Science and Technology*, NATO ASI Series E, No. 80; Ribeiro, F. R., Rodrigues, A. E., Rollmann, L. D., Naccache, C., Eds.; Martinus Nijhoff Publishers: The Hague, 1984; p 529.
(6) Haag, W. O.; Lago, R. M.; Weisz, P. B. *Nature (London)* **1984**, *309*, 589.

S0002-7863(97)02903-X CCC: $15.00
Published on Web 02/06/1998

Scheme 1

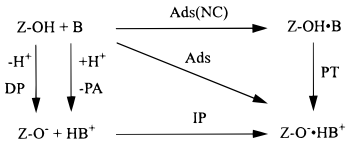

Hallam−Williams relation[7]). The results depend on details of the procedure such as which molecules are selected as base molecules and reference acids (see Table 18 of ref 8 and the references therein).

Another way of characterizing the acid strength of solid acids is measuring the heat of adsorption of ammonia by microcalorimetry (MC) or temperature-programmed desorption (TPD).[9] On adsorption of NH_3 on sites of sufficient acid strength, the acidic proton is transferred onto ammonia and ammonium ions are formed which, unlike the proton-transfer products in the gas phase, interact with the negatively charged surface site of the catalyst.[10−13] Hence, the energy of adsorption of NH_3 depends not only on the energy of deprotonation of the solid acid (DP), but also on the proton affinity of NH_3 (PA) and the binding energy of the ammonium ion onto the negatively charged surface (ion pair binding energy IP), as shown in the thermodynamic cycle in Scheme 1. Z stands for zeolite, the class of solid acids studied here.

While the proton affinity of NH_3 is a constant when measuring the heat of NH_3 adsorption on different catalysts, this cannot be assumed for the interaction of the NH_4^+ ion with the negatively charged surface. Hence, the heat of NH_3 adsorption may yield an acidity scale for solid acids which is different from that based on the heat of deprotonation.

In contrast with experiments, quantum chemical ab initio calculations provide a direct access to heats of deprotonation also for surface hydroxyl groups.[14] Heats of NH_3 adsorption can also be calculated and comparison can be made between the two different measures of acid strength. For molecules in the gas phase, such calculations became routine in the past decade.[2,3] For acidic sites of solid acids, until recently, quantum chemical ab initio calculations were feasible only when replacing the solid by a finite model of its active site.[15] Although these calculations contributed substantially to our knowledge of, e.g., zeolite acidity,[15−28] their limitation is that they cannot discriminate between the acidities of Brønsted sites in different crystallographic environments. They lack the structure constraint by and the long-range influence of the extended solid. This limitation can be overcome only if the periodic crystal structure is included in the theoretical model. In principle, periodic boundary conditions could be imposed which reduce the size of the problem to the size of a repeating cell of the crystal. Due to the large size of the unit cell and broken point symmetry if Brønsted sites are present, such calculations are still exceptional and limited to framework types with a small number of atoms in the unit cell. Periodic Hartree−Fock calculations using the CRYSTAL code[29] have been reported for acidic zeolites with small unit cells only (chabazite, sodalite), few structure parameters have been optimized, and small basis sets without polarization functions have been used.[30,31] Periodic density functional calculations employing plane waves as basis sets find increasing use for zeolites,[32−34] but their application to a series of zeolite structures with unit cells as large as ZSM-5 is still computationally very demanding.

We use an alternative technique[35] that combines a quantum mechanical ab initio treatment (QM) of a finite size model of the active site with a description of the periodic zeolite structure and its interaction with the active site by an interionic shell model potential (Pot). The approach is fully ab initio in the sense that the parameters of the shell model potential are parametrized on ab initio data of finite size models for Brønsted sites of zeolites[36] and their complexes with ammonia and the ammonium ion.[37] This combined QM-Pot method proved successful in determining the structures of dense and microporous silica polymorphs,[35] the structures, spectroscopic properties, and the heats of deprotonation of Brønsted sites in zeolites H-faujasite and H-ZSM-5,[8] and the heat of NH_3 adsorption in H-faujasite[37] and H-chabazite.[38] Here, we report results for mordenite (MOR) and ZSM-5 (MFI), two widely employed catalysts, and compare them with results for faujasite (FAU)[37] and chabazite (CHA)[38] obtained in exactly the same way. This study, for the first time, makes theoretical predictions of absolute acidites of a series of different zeolites. Heats of deprotonation are calculated which are important benchmarks for data obtained by the Bellamy−Hallam−Williams relations and which allow one to put surface hydroxyls on the same

(7) Bellamy, L. J.; Hallam, H. E.; Williams, R. E. *Trans. Faraday Soc.* **1958**, *54*, 1120.
(8) Eichler, U.; Brändle, M.; Sauer, J. *J. Phys. Chem. B* **1997**, *101*, 10035.
(9) Farneth, W. E.; Gorte, R. J. *Chem. Rev.* **1995**, *95*, 615.
(10) Blumenfeld, A. L.; Coster, D.; Fripiat, J. J. *J. Phys. Chem.* **1995**, *99*, 15181.
(11) Jacobs, W. P. J. H.; de Haan, J. L.; van den Ven, L. J. M.; van Santen, R. A. *J. Phys. Chem.* **1993**, *97*, 10394.
(12) Jacobs, W. P. J. H.; van Wolput, J. H. M. C.; van Santen, R. A. *Zeolites* **1993**, *13*, 170.
(13) Uytterhoeven, J. B.; Christner, L. G.; Hall, W. K. *J. Phys. Chem.* **1965**, *69*, 2117.
(14) Sauer, J. *J. Mol. Catal.*, **1989**, *54*, 312.
(15) Sauer, J. *Chem. Rev.* **1989**, *89*, 199.
(16) Sauer, J.; Ugliengo, P.; Garrone, E.; Saunders, V. R. *Chem. Rev.* **1994**, *94*, 2095.
(17) Gale, J. D. *Top. Catal.* **1996**, *3*, 169.
(18) Krossner, M.; Sauer, J. *J. Phys. Chem.* **1996**, *100*, 6199.
(19) Haase, F.; Sauer, J. *J. Am. Chem. Soc.* **1995**, *117*, 3780.
(20) Van Santen, R. A.; Kramer, G. J. *Chem. Rev.* **1995**, *95*, 637.
(21) Haase, F.; Sauer, J. *J. Phys. Chem.* **1994**, *98*, 3083.
(22) Sauer, J. In *Zeolites and Related Microporous Materials: State of the Art 1994*; Weitkamp, J., Karge, H. G., Pfeifer, H., Hölderich, W., Eds. *Stud. Surf. Sci. Catal.* **1994**, *84*, 2039.
(23) Teunissen, E. H.; van Santen, R. A.; Jansen, A. P. J.; van Duijneveldt, F. B. *J. Phys. Chem.* **1993**, *97*, 203.
(24) Kassab, E.; Fouquet, J.; Allavena, M.; Evleth, E. M. *J. Phys. Chem.* **1993**, *97*, 9034.
(25) Sauer, J.; Kölmel, C.; Haase, F.; Ahlrichs, R. In *Proceedings of the 9th International Zeolite Conference, Montreal 1992*; v. Ballmoos, R., Higgins, J. B., Treacy, M. M. J., Eds.; Butterworth-Heinemann: Boston, 1993; p 679.
(26) Brand, H. V.; Curtiss, L. A.; Iton, L. E. *J. Phys. Chem.* **1993**, *97*, 12773.
(27) Brand, H. V.; Curtiss, L. A.; Iton, L. E. *J. Phys. Chem.* **1992**, *96*, 7725.
(28) Sauer, J. In *Molecular Modelling of Structure and Reactivity in Zeolites*; Catlow, C. R. A., Ed.; Academic Press: London, 1992; p 183.
(29) (a) Pisani, C.; Dovesi, R.; Roetti, C. *Hartree-Fock Ab Initio Treatment of Crystalline Systems*, Lecture Notes in Chemistry, Vol. 48; Springer-Verlag: Berlin, 1988. (b) Roetti, C. In *Quantum-Mechanical Ab-initio Calculations of the Properties of Crystalline Materials*; Lecture Notes in Chemistry, Vol. 67; Pisani, C., Ed.; Springer-Verlag: Berlin, 1996; p 125.
(30) Teunissen, E. H.; Roetti, C.; Pisani, C.; de Man, A. J. M.; Jansen, A. P. J.; Orlando, R.; van Santen, R. A.; Dovesi, R. *Mod. Simul. Mater. Sci. Eng.* **1994**, *2*, 921.
(31) Nicholas, J. B.; Hess, A. C. *J. Am. Chem. Soc.* **1994**, *116*, 5428.
(32) Nusterer, E.; Blöchl, P. E.; Schwarz, K. *Angew. Chem.* **1996**, *108*, 187.
(33) Shah, R.; Gale, J. D.; Payne, M. C. *J. Phys. Chem.* **1996**, *100*, 11688.
(34) Haase, F.; Sauer, J.; Hutter, J. *Chem. Phys. Lett.* **1997**, *266*, 397.
(35) Eichler, U.; Kölmel, C. M.; Sauer, J. *J. Comput. Chem.* **1997**, *18*, 463.
(36) Schröder, K.-P.; Sauer, J. *J. Phys. Chem.* **1996**, *100*, 11043.
(37) Brändle, M.; Sauer, J. *J. Mol. Catal. A: Chemical* **1997**, *119*, 19.
(38) Brändle, M.; Sauer, J.; Dovesi, R.; Harrison, N. In preparation.

acidity scale as gas-phase molecules. In addition, heats of ammonia adsorption are calculated for the same set of systems. It will be shown that these two different measures of acidity yield different acidity sequences for the four different zeolites considered. The calculations are all made for high Si/Al ratios which permits the study of isolated Brønsted sites. For some zeolites, e.g., for faujasite, such samples are difficult to prepare experimentally. The difference in the Si/Al ratios of common zeolite catalysts such as HY and H-ZSM-5 is one of the main factors which hampers the comparison of the acidities of their Brønsted sites. It is one of the advantages of the theoretical approach that data can be predicted that are difficult to obtain experimentally. It is possible to separate the influence of different parameters on the acidity of zeolite catalysts such as framework structure (investigated in this study) and Si/Al ratio (investigated in another study[39]). This study is limited to crystalline materials, but the method presented is easily applicable to Brønsted sites in amorphous or mesoporous materials.[40]

We proceed as follows. We summarize the basic features of the combined QM-Pot scheme in the Method's section, which also includes comparison with previous attempts[41,42] to improve the cluster model and gives all technical details. We then explain for all frameworks studied which crystallographic sites are selected as Brønsted sites (section 3). Our criterion is the lowest lattice energy. We add the ammonia molecule to the protonated system and the ammonium ion to the deprotonated system, perform lattice energy minimizations using the ab initio parametrized interionic shell model potential alone, and obtain initial structures of the neutral and ion-pair adsorption structures (section 4). The results guide us in designing the cluster models for use in the embedded cluster scheme (section 5). We then perform embedded cluster structure optimizations by the QM-Pot method for the protonated and deprotonated systems and calculate the energy of deprotonation from the total energies obtained. Structure optimizations for the neutral complex, Z−OH·NH_3, and the ion-pair complex, Z−O^-·NH_4^+, yield total energies from which the energy of adsorption is calculated. The final heats of deprotonation and adsorption are obtained after adding corrections for the electron correlation and nuclear motion effects at finite temperature. All this is presented in the Results and Discussion (section 6) which also includes a test of our results by increasing the size of our embedded cluster models (section 6.3). Comparison between the four framework types is made in section 6.5, and section 6.6 provides comparison with experimental data available.

2. Method

2.1. The Combined QM-Pot Method. The embedding scheme[35] we use decomposes the energy of the entire system (S) into contributions of the inner part (I) containing the active site, the outer part (O), and an interaction term (I−O). Only the inner part is treated quantum mechanically. The remaining contributions are described at the level of interatomic potential functions:

$$E_{\mathrm{QM-Pot}}(\mathrm{S}) = E_{\mathrm{QM}}(\mathrm{I}) + E_{\mathrm{Pot}}(\mathrm{O}) + E_{\mathrm{Pot}}(\mathrm{O-I}) \quad (1)$$

In practice the equivalent subtraction scheme

$$E_{\mathrm{QM-Pot}}(\mathrm{S}) = E_{\mathrm{QM}}(\mathrm{I}) + E_{\mathrm{Pot}}(\mathrm{S}) - E_{\mathrm{Pot}}(\mathrm{I}) \quad (2)$$

is used, which involves only energies that can be obtained from straightforward application of available codes to well-defined systems. For a given cluster of a given system, $E_{\mathrm{QM-Pot}}(\mathrm{S})$ differs from $E_{\mathrm{QM}}(\mathrm{S})$ by a constant which describes the difference between the energy scales of QM and Pot.

If the inner part is chemically bonded to the outer region, the cut between inner and outer part creates dangling bonds which have to be terminated by H atoms, also called link atoms, L. The link atoms and the inner part form the cluster, C = I + L. The energy of the total system can still be approximated by the subtraction scheme,

$$E_{\mathrm{QM-Pot}}(\mathrm{S}) = E_{\mathrm{QM}}(\mathrm{C}) + E_{\mathrm{Pot}}(\mathrm{S}) - E_{\mathrm{Pot}}(\mathrm{C}) \quad (3)$$

if it is assumed that

$$\Delta = -E_{\mathrm{QM}}(\mathrm{L}) - E_{\mathrm{QM}}(\mathrm{L-I}) + E_{\mathrm{Pot}}(\mathrm{L}) + E_{\mathrm{Pot}}(\mathrm{L-I}) \quad (4)$$

is zero. Hence, the subtraction scheme eliminates approximately the contribution from the terminating atoms which are not part of the real solid. The difference Δ will be the smaller the better the interatomic potential function mimicks the quantum mechanical potential energy surface for the cluster. Parameters for interatomic potentials describing the cluster including its link atoms are needed to evaluate $E_{\mathrm{Pot}}(\mathrm{C})$, but are generally not available from empirical sources. Therefore, the use of potential functions fitted to ab initio data becomes necessary. In this study we use the Hartree−Fock method for the QM part and a Hartree−Fock parametrized shell model potential for zeolites[36] and their interaction with NH_3 and NH_4^+.[37] The same basis sets are used for the QM part and the shell model parametrization. The dipolar shell model introduced by Dick and Overhauser[43] accounts for the polarization of the anions in an electric field. In silicates and zeolites the O^{2-} ion is represented by a pair of point charges, the positive core, and the negative massless shell which are connected by a harmonic spring. The sum of the core and shell charges is the formal charge of the anion. Formal charges were used for all ions. In addition, the present potential functions include nondirectional two-body Born-Mayer repulsion and three-body angle bending terms.

Note that there is no direct influence of the charge distribution of the outer part on the wave function of the cluster. The latter is different from the wave function of the gas-phase cluster only by way of the structure changes that the cluster experiences when it is embedded in the outer part. However, the energy lowering due to the mutual polarization of the inner and the outer parts is included at the level of the interatomic potential function (shell model potential). The forces on the nuclei used for structure optimization are obtained as

$$F_{\alpha,\mathrm{QM-Pot}}(\mathrm{S}) = F_{\alpha,\mathrm{QM}}(\mathrm{C}) + F_{\alpha,\mathrm{Pot}}(\mathrm{S}) - F_{\alpha,\mathrm{Pot}}(\mathrm{C}) \quad \alpha \in \mathrm{I} \quad (5)$$

$$F_{\beta,\mathrm{QM-Pot}}(\mathrm{S}) = F_{\beta,\mathrm{Pot}}(\mathrm{S}) \quad \beta \in \mathrm{O} \quad (6)$$

The terminating atoms are not moved independently, but their positions are given by the positions of the atoms of the corresponding bond in the crystal. This creates additional contributions to the forces on these atoms.[35] Equation 5 shows

(39) Sierka, M.; Datka, J.; Sauer, J. In preparation.

(40) Liepold, A.; Roos, K.; Reschetilowski, W.; Schmidt, R.; Stöcker, M.; Philippou, A.; Anderson, M. W.; Esculcas, A. P.; Rocha, J. In *Progress in Zeolite and Microporous Materials*; Chon, H., Ihm, S.-K., Uh, Y. S., Eds. *Stud. Surf. Sci. Catal.* **1997**, *105*, 423.

(41) Greatbanks, S. P.; Sherwood, P.; Hillier, I. H. *J. Phys. Chem.* **1994**, *98*, 8134.

(42) Greatbanks, S. P.; Sherwood, P.; Hillier, I. H.; Hall, R. J.; Burton, N. A.; Gould, I. R. *Chem. Phys. Lett.* **1995**, *234*, 367.

(43) Dick, Jr., B. G.; Overhauser, A. W. *Phys. Rev.* **1958**, *112*, 90.

that the periodic zeolite structure has a direct influence on the forces of the active site atoms ($\alpha \in$ I). For the same active site cluster, different zeolite frameworks lead to different local structures for the Brønsted site. For this reason, we refer to the combined QM-Pot scheme sometimes as "mechanical" embedding.

The reaction energy for a general reaction R → P can be expressed as

$$\Delta E_{\mathrm{QM-Pot}} = \Delta E_{\mathrm{QM}} + \Delta E_{\mathrm{Pot}} \tag{7}$$

with

$$\Delta E_{\mathrm{QM}} = E_{\mathrm{QM}}(\mathrm{C_P}) - E_{\mathrm{QM}}(\mathrm{C_R}) \tag{8}$$

and, assuming $\Delta = 0$,

$$\Delta E_{\mathrm{Pot}} = E_{\mathrm{Pot}}((\mathrm{O-I})_{\mathrm{P}}) - E_{\mathrm{Pot}}((\mathrm{O-I})_{\mathrm{R}}) + E_{\mathrm{Pot}}(\mathrm{O_P}) - E_{\mathrm{Pot}}(\mathrm{O_R}) \tag{9}$$

Subscripts R and P refer to reactants and products, respectively. If the cluster is chosen such that the reaction changes the inner part of the system only, and if we further assume that the structure of the outer part is about the same for P and R, $E_{\mathrm{Pot}}(\mathrm{O_P}) - E_{\mathrm{Pot}}(\mathrm{O_R})$ approximately vanishes and

$$\Delta E_{\mathrm{Pot}} \approx E_{\mathrm{Pot}}((\mathrm{O-I})_{\mathrm{P}}) - E_{\mathrm{Pot}}((\mathrm{O-I})_{\mathrm{R}}) \tag{10}$$

If the cluster is large enough that all short-range terms of the interatomic potentials vanish between the active site and the cluster boundary, only long-range (lr) terms remain in eq (10), and we can write

$$\Delta E_{\mathrm{Pot}} \approx E_{\mathrm{lr}} \tag{11}$$

and

$$\Delta E_{\mathrm{QM-Pot}} = \Delta E_{\mathrm{QM//QM-Pot}} + \Delta E_{\mathrm{lr//QM-Pot}} \tag{12}$$

The notation "//QM-Pot" means "at the structure obtained by the combined QM-Pot method". For brevity, we use "QM-Pot" instead of "QM-Pot//QM-Pot". Equation 12 reflects that the combined QM-Pot approach has two effects on the reaction energies.

(i) The quantum mechanical contribution to the reaction energy is calculated for cluster models of the reactants and products at the structures that have been obtained by the combined QM-Pot approach. Compared to gas-phase clusters, the structure relaxation is limited by framework constraints. The framework constraints are framework specific. This means that for the same reaction and the same cluster size $\Delta E_{\mathrm{QM//QM-Pot}}$ is different for different zeolites.

(ii) The interatomic potential functions describing the interaction between the inner and the outer region provide a long-range correction to the calculated reaction energy. The shell model allows for mutual polarization of the reaction site and the periodic environment.

For the comparison of the predicted reaction energies with experiment, electron correlation, zero-point energy, and thermal effects must be accounted for. These are included a posteriori by MP2 calculations on molecular models at the structures obtained by the embedding scheme at the Hartree-Fock level.

The reliability of the energies that the QM-Pot scheme yields can be checked either by use of models of equal size embedded differently at symmetry equivalent positions or by use of models of increasing size, always embedded at the same position. From test calculations on di-tetrahedra clusters embedded differently at symmetry equivalent positions in the faujasite[8,35] and chabazite[38] structures, its accuracy is known to be better than 2.5 kJ/mol. This is within chemical accuracy. This study includes checks of the convergence by using models of increasing size for the same site.

Greatbanks et al. developed a different embedded cluster scheme[41] and applied it to adsorption of ammonia in faujasite.[42] A finite set of point charges is fitted to the periodic electrostatic potential of the siliceous zeolite for a given structure. This potential is added to the Hamiltonian of the tri-tetrahedra cluster used. Structure relaxation is limited to the $AlO_4(H)$ core and the adsorbed NH_3 and polarization of the embedding framework is not included. Comparisons of different frameworks have not been performed so far. For further details and comparison with additional studies we refer to ref 37.

2.2. Technical Details. We use an implementation of the QM-Pot scheme[35] that couples the quantum chemical code TURBOMOLE[44] with the General Utility Lattice Program (GULP)[45] for periodic calculations using interatomic potentials. The quantum mechanical (QM) calculations for the embedded cluster adopt the Hartree−Fock approximation. Double-ζ basis sets are used for silicon, aluminum, and hydrogen atoms. For the oxygen and nitrogen atoms a valence triple-ζ basis set was employed. For the Si, Al/O, N/H atoms Huzinaga's[46,47] (11s,7p)/(9s,5p)/(4s) primitive sets are contracted as {521111, 4111}/{51111, 311}/{31}. Polarization functions are added to all atoms; the exponents are 0.4 (Si), 0.3 (Al), 1.2 (O), 1.0 (N), and 0.8 (H). This is the basis set used in many previous studies on zeolites from this laboratory; see, e.g., refs 16, 19, 22, 25, and 28. It is denoted T(O,N)DZP. The cluster models are defined such that they terminate with OH groups. The OH groups bonded to a silicon/aluminum atom have a fixed link atom distance r_{OH} of 94.5/94.0 pm obtained by free cluster optimizations with the same basis set. All SCF calculations were carried out in C_1 symmetry.

Before optimizations using the combined QM-Pot scheme are made, it is convenient to optimize first both the ion and shell positions of the entire system in constant pressure mode with the shell model potential only. This has the advantage that the positions of the atoms in the outer region are already relaxed and, therefore, optimization cycles can be saved in the following QM-Pot part. In addition, preferred adsorbate positions can be localized at low computational expense. The present implementation of the QM-Pot scheme uses constant volume optimizations and does not exploit space group symmetry. An energy threshold of 0.01 kJ/mol is taken as the convergence criterion. The electrostatic energy is evaluated by standard Ewald summation techniques for all cores and shells. A cut-off radius of 10 Å is chosen for the summation of short-range interactions.

The embedded cluster calculations assume a periodic array of active sites or surface complexes. In the case of deprotonated zeolites, the excess charge occurring in each unit cell for the periodic system was neutralized by immersing the framework into a homogeneous background charge distribution. To obtain deprotonation energies with respect to removal of a single proton in an otherwise periodic array of bridging hydroxyl groups and

(44) Ahlrichs, R.; Bär, M.; Häser, M.; Horn, H.; Kölmel, C. Program TURBOMOLE. *Chem. Phys. Lett.* **1989**, *162*, 165. TURBOMOLE is commercially available from Molecular Simulations Inc., San Diego, CA.

(45) Gale, J. D. *J. Chem. Soc., Faraday Trans.*, **1997**, *93*, 629.

(46) Huzinaga, S. *Approximate Atomic Wavefunctions I, II*; University of Alberta: Edmonton, 1971.

(47) Huzinaga, S. *J. Chem. Phys.* **1965**, *42*, 1293.

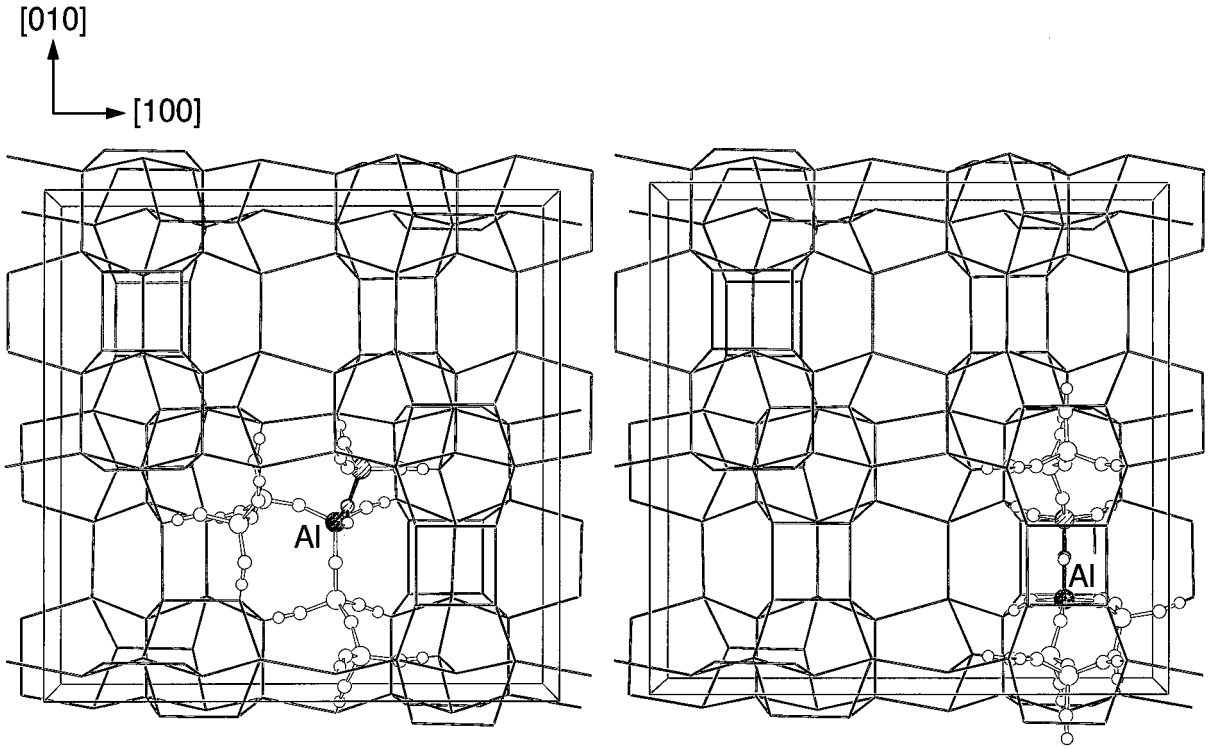

Figure 1. Framework of zeolite H-ZSM-5. Shaded atoms: Bridging hydroxyl groups of the REG (left unit cell, Al7−O17(H)−Si4) and the CIS (right unit cell, Al12−O24(H)−Si12) positions. Also shown: 6-tetrahedra models embedded at these positions.

ion-pair binding energies with respect to the removal of a single ammonium ion, the interaction between these species in the repeating cell has to be removed. This is achieved by adding a macroscopic estimate for the interaction of charged defects in a lattice[48] as described in ref 8. Both the approximations for the ion-pair binding and the deprotonation energy introduce a deviation of ±2 kJ/mol for the sum of the QM-Pot reaction energies over the complete thermodynamic cycle of Scheme 1.

3. Localization of Brønsted Sites

MFI. The MFI framework of ZSM-5 consists of intercrossing straight channels in the [010] and sinusoidal channels in the [100] direction.[49] The high-silica form, silicalite, occurs in two modifications of different symmetry. Below 340 K the low-temperature monoclinic form (space group $P2_1/n.1.1$, asymmetric unit $T_{24}O_{48}$) is the most stable one.[50] A Brønsted site can be created by substitution of Si with (Al,H) at 96 different bridging hydroxyl positions. Previous calculations using an empirical shell model potential on all 96 different O positions revealed that the Al7−O17(H)-Si4 and Al19-O43(H)-Si4 bridging hydroxyl sites (numbering according to ref 50) are the most stable ones.[51] We study here the orthorhombic form (space group *Pnma*, asymmetric unit $T_{24}O_{48}$)[52] that ZSM-5 assumes above 340 K or at loadings with adsorbates. In this modification the two positions are related by symmetry and join to the Al7-O17(H)-Si4 position which we will call the "regular" site (REG). An earlier QM cluster study by Brand et al. considered the T12-O24-T12 and T2-O13-T8 sites (crystallographic position numbering according to high-temperature structure).[26,27] The reason for this choice was their easy accessibility at the intersection of the two channel systems and in the straight channel, respectively. Lattice energy minimizations with the empirical shell model showed that both sites are less stable than the REG site.[51] Combined QM-Pot calculations on embedded di-tetrahedra clusters confirmed that the Al12-O24(H)-Si12 site is by 10.6 kJ/mol less stable than the REG site.[8] Here we study ammonia adsorption on the most stable Al7-O17(H)-Si4 site and, for comparison, also present results for the Al12-O24(H)-Si12 site which we call the "channel intersection" position (CIS). Figure 1 shows the location of the two sites studied in the MFI framework.

MOR. Figure 2 shows the mordenite framework. The main channel in the [001] direction consists of 12-rings and is connected with 8-ring side pockets in the [010] direction.[49] For the labeling of the T atom sites (T = Si, Al) we follow Alberti et al.[53] This single-crystal X-ray determination assumed the orthorhombic space group $Cmc2_1$. However, the zeolite framework possesses the higher space group *Cmcm*. The composition of the asymmetric unit is T_4O_{10}. The extension of the unit cell in the *c* direction is quite small, 7.5 Å. To avoid problems with embedding the cluster (vide infra) and also to be able to fine-tune the Si/Al ratio, we use a larger supercell. The conventional unit cell was first reduced from the *C* face-centered symmetry to a primitive unit cell with space group $P2_1/m$, unique axis *b*. Then, the lattice constant of this primitive unit cell in the direction of the main channel was doubled. The composition of this supercell is $T_{48}O_{96}$. The relation between the conventional cell and the supercell used is shown in Figure 2. Substituting one aluminum atom for a silicon atom yields a catalyst with an Si/Al ratio of 47.

There are 14 different possibilities to create a Brønsted site by introducing the Al atom in the four different T sites and by

(48) Leslie, M.; Gillan, M. J. *J. Phys. C.: Solid State Phys.* **1985**, *18*, 973.

(49) Meier, W. M.; Olson, D. H. *Atlas of Zeolite Structure Types*, 2nd rev. ed.; Butterworths: London, 1987.

(50) Van Koningsveld, H.; Jansen, J. C.; van Bekkum, H. *Zeolites* **1990**, *10*, 235.

(51) Schröder, K.-P.; Sauer, J.; Leslie, M.; Catlow, C. R. A. *Zeolites* **1992**, *12*, 20.

(52) Van Koningsveld, H. *Acta Crystallogr. B* **1990**, *46*, 731.

(53) Alberti, A.; Davoli, P.; Vezzalini, G. Z. *Kristallogr.* **1986**, *175*, 249.

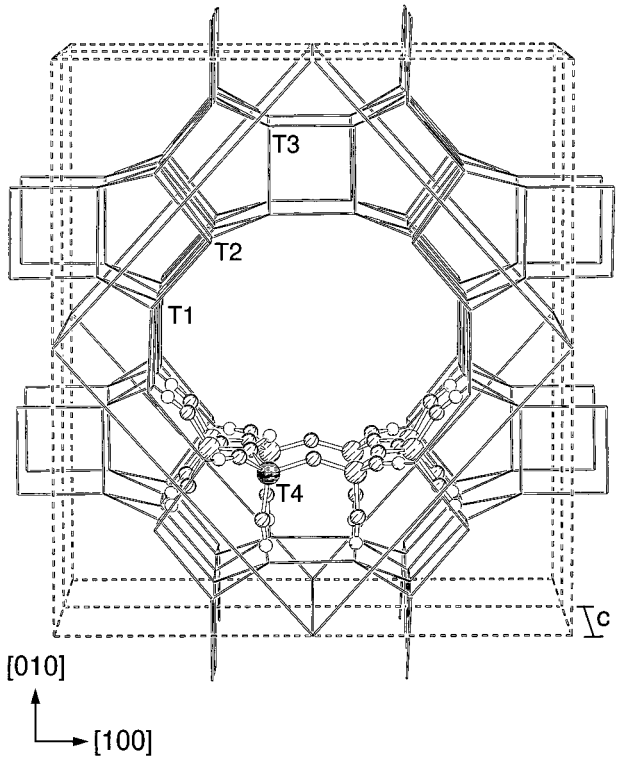

Figure 2. Mordenite framework showing used T (T=Si,Al) atom numbering.[53] View along main channel. Dashed box: C-centred conventional unit cell. Solid box: Primitive unit cell. The cell boxes are doubled in [001] direction. Also shown: 8-ring model embedded around side pocket.

adding a proton to the crystallographically distinct oxygen positions. Lattice energy minimizations were performed for all 14 structures. As for zeolite ZSM-5,[51] the energy differences between these structures are small, between 0 and 18 kJ/mol. The energies of the two most stable ones, Al4-O2(H)-Si and Al2-O6(H)-Si, differ by 1 kJ/mol only. These two positions were investigated further. Combined QM-Pot optimizations on embedded di-tetrahedra models showed that O2(H) is stabilized by 6.6 kJ/mol with respect to O6(H). Therefore we decided to continue with the Al4-O2(H)-Si site only.

The structures of the deprotonated MOR catalysts were determined by lattice energy minimizations for the four different Al positions. The energy order obtained, T4 < T2 < T1 < T3, indicates that Al occupies preferentially the T4 position in the four-membered ring. However, the energy differences are small again. Al is less stable in T3 than in T4 by 4.4 kJ/mol only.

4. Determination of Initial Structures

In this section we report the structures which are obtained by lattice energy minimizations using the shell model potential only. These structures serve as initial guess in the structure determination using the QM-Pot method. In some cases the initial structures are different from the final QM-Pot result. We report them both since comparison of the initial and final structures allows a judgment of the quality of our shell model potential functions.

MFI. The structures optimized by means of the shell model potential for the ammonia complexes NH_3·H-ZSM-5, show a 2-fold coordination of NH_3 to the surface. Ammonia accepts a hydrogen bond from the surface OH groups (O17 and O24 for REG and CIS, respectively) and donates a hydrogen bond to the framework oxygen atoms (O23 and O20 for REG and CIS, respectively). The two oxygen atoms involved in these surface bonds belong to the AlO_4^- tetrahedron. The structures optimized for the ammonium forms of ZSM-5, NH_4^+ZSM-5$^-$, show a 3-fold coordination of NH_4^+ (O17, O23, O26 and O24, O20, O11 for REG and CIS, respectively). Independent of the presence of the adsorbate and of the location of the Brønsted site (REG or CIS), the lattice constants of all the frameworks vary only slightly: a = 20.42−20.43 Å, b = 20.19−20.25 Å, c = 13.62−13.65 Å; α = 89.9−90.1°, β = 89.9−90.1°, γ = 90.0−90.1°.[54] This indicates that the distortions induced by coupling of an adsorbate to an active site are only local and easily accommodated by the framework.

MOR. Two different minimum structures of NH_4^+ attached to the AlO_4^- tetrahedron were found in the optimizations by means of the shell model potential. In one of them, NH_4^+ was in the main channel and 3-fold coordinated to O2, O2″, and O10 (cf. Figure 5). In the other one, NH_4^+ was in the main channel above the side pocket and 2-fold coordinated to O2 and O10 (cf. Figure 5). Since single-point QM-Pot calculations yielded a lower energy for the latter structure, it was used as the initial structure in QM-Pot optimizations. NH_3 was attached to the O2-H and O10-H sites and the resulting structures were optimized. For all structures used as initial guess in the following QM-Pot calculations, the lattice constants of the MOR frameworks vary only slightly: a = 13.75−13.77 Å, b = 15.15−15.18 Å, c = 13.74−13.77 Å; α = 89.8−90.0°, β = 83.7−84.1°, γ = 90.0−90.2°.[54]

The final NH_4^+ adsorption structures reported below (Figures 3−5) and obtained with the combined QM-Pot method are different from the initial structures obtained with the shell model potential alone. Three-fold coordination is changed to 2-fold coordination (CIS position in ZSM-5), and 2-fold coordination to O atoms of one AlO_4^- tetrahedron is changed to 2-fold coordination across a ring (side pocket of MOR, Figure 5). This shows that the shell model potential developed for NH_4^+ ion − zeolite interaction is better suited for situations where only two-coordination is possible, such as occurs in large pore zeolites. For small pore zeolites it is important that all possible short-range interactions between an adsorbate and the zeolite framework are included in the QM cluster.

5. Embedded Models

In this study we use two classes of embedded cluster models. The standard models are used for structure determination and energy evaluation of all forms of the catalyst involved in Scheme 1. The extended models are used for checking the convergence of the combined QM-Pot scheme with increasing cluster size.

Standard Models. Clusters as small as two tetrahedra are sufficient for use in the combined QM-Pot scheme when deprotonation energies are calculated. However, when calculating also heats of NH_3 adsorption they must be designed such that all relevant short-range interactions between the adsorbate and the surrounding framework are included in the QM part. All oxygen atoms have to be considered which are possible candidates for hydrogen bonds of the adsorbate, since these bonds are difficult to model by a shell model potential alone. In general, a compromise between the size of the cluster (and concomitant computational cost) and the number and range of zeolite−adsorbate interactions treated by the QM part must be found. Total QM-Pot energies of different adsorption positions can only be compared if clusters of the same size are embedded.

In the initial structures determined for the REG and CIS positions of NH_4-ZSM-5, the NH_4^+ ion forms close contacts to

(54) The detailed lattice constants of the MFI and MOR frameworks obtained by lattice energy minimizations can be accessed as Supporting Information in the electronic supporting information of this journal.

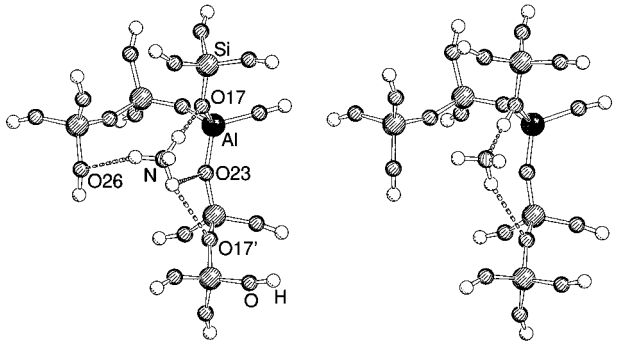

Figure 3. 6-Tetrahedra models of NH_3·H−ZSM-5 and NH_4^+·ZSM-5^- embedded at the REG position. Structures optimized with the combined QM-Pot scheme. Similar models were adopted for H-ZSM-5 and its deprotonated form.

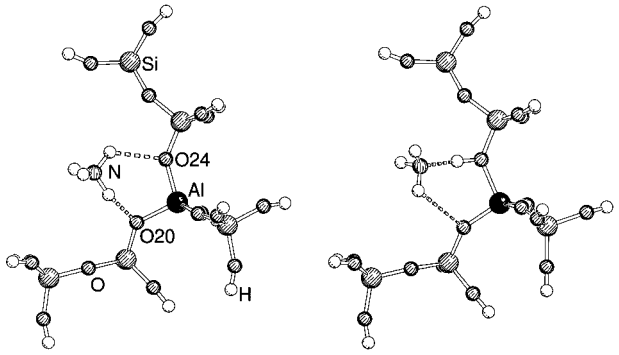

Figure 4. 6-Tetrahedra models of NH_3·H−ZSM-5 and NH_4^+·ZSM-5^- embedded at the CIS position. Structures optimized with the combined QM-Pot scheme. Similar models were adopted for H-ZSM-5 and its deprotonated form.

at least two oxygen atoms. We consider branched models of 6-tetrahedra as appropriate and embed them at both the REG and the CIS positions; see Figure 1. Figures 3 and 4 show these 6T models loaded with NH_3 and NH_4^+, respectively.

To include all possible close interactions of the adsorbates with the mordenite framework in the QM part, we embedded 8-ring models at the side pocket around the O2-Al4-O10 group; see Figure 2. This choice is similar to our study[38] of NH_3 adsorption in the high-silica chabazite structure, which possesses also small pores of 8-rings. In the case of the neutral complex and the protonated zeolite, we investigated the two proton positions O2-H and O10-H, both with Al at position T4. Figure 5 shows the structures of the adsorbate complexes.

Extended Models. For these clusters we did not optimize the structure but performed "single point" calculations at the structures obtained when embedding the 6T or 8R models. The design of cluster models of increasing size is not completely free. We define the formal composition of an OH terminated model without adsorbate and without the bridging hydroxyl proton as T_mO_{2m}, with $m = n(\mathrm{T}) + 0.25n(\mathrm{H})$. n(T) is the number of T atoms actually present in the model; n(H) is the number of terminating H atoms which represent a quarter of the T atom of the periodic structure they replace.[15] The maximum size of the T_mO_{2m} cluster is limited by the formal composition of the zeolite unit cell T_nO_{2n}, $m \leq n$. A stronger condition is that the extension of the cluster along a given unit cell direction must not be larger than the translational period in this direction. The reason is clear from Scheme 2. At left, a cluster is shown (oval) which is smaller than the unit cell (square) of the periodic embedding lattice. The periodic calculation of the total system S evaluates the energy per unit cell as sum over all interactions between the atoms in a reference

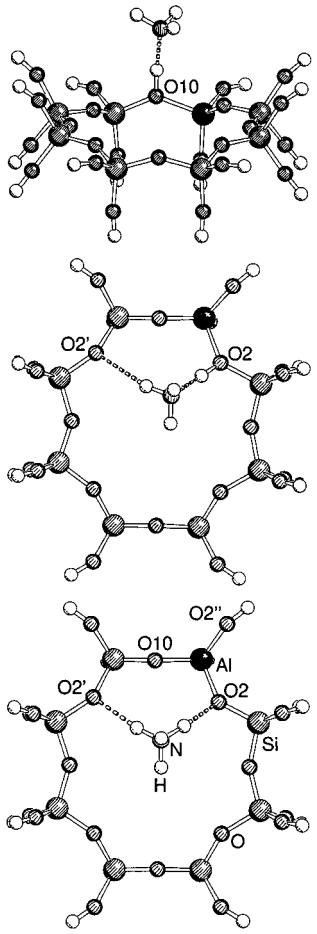

Figure 5. 8-Ring models of NH_3·H-MOR and NH_4^+·MOR^- embedded at the side pocket. Structures optimized with the combined QM-POT scheme. Similar models were adopted for H-MOR and its deprotonated form.

Scheme 2

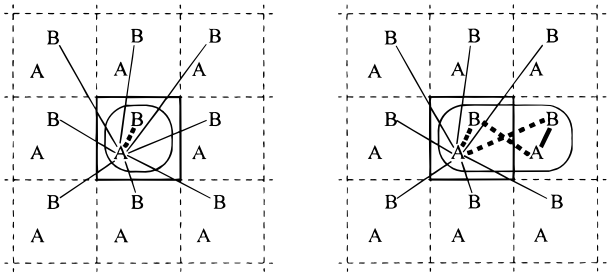

cell with all surrounding atoms, exemplified here for the interaction of an atom A in the reference cell with all surrounding atoms B. The embedded model describes only the interaction A−B in the reference cell. In the QM-Pot scheme this interaction is subtracted (visualized by a bold dashed line) from the host energy. If the cluster is extended in one direction over the translational period of the unit cell, shown right, it will contain the interactions between the atoms repeated by the translation twice (bold line). In this case, supercells have to be used in the QM-Pot scheme. Moreover, one has to make sure that the number of reaction centers included in the model is also doubled when doubling the primitive cell. If not, QM and Pot reaction energies for the clusters extended too far cannot be compared with the converged periodic value; they rather converge to a value which corresponds to dilution of the reaction center. Such situations occur in several recent investigations of the energy dependence on cluster size.[26,30]

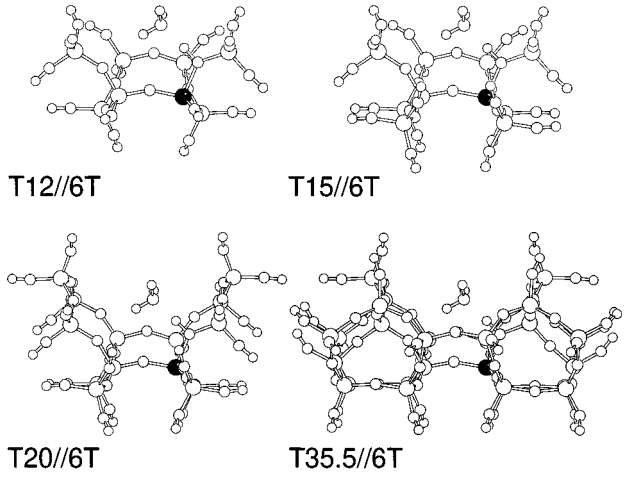

Figure 6. Clusters of increasing size embedded in NH_3·H−ZSM-5, REG position (Al7−O17−Si4). Similar models were embedded in NH_4^+·ZSM-5^-, H-ZSM-5 and its deprotonated form.

Moreover, when constructing larger embedded models, situations have to be avoided in which two terminating hydroxyl groups are pointing to the same silicon atom of the outer region, since their close interaction is not parametrized by the present shell model potential. In such a case the silicon atom was also used in the cluster description and terminated with hydroxyl groups.

ZSM-5. The extension of cluster models in ZSM-5 is limited by the shortest unit cell length, here in *c* direction. Using a single primitive cell only, it is not possible to build models which include the whole 10-ring pore without violating the conditions discussed before. For the REG position, the QM-Pot optimized 6T model was first completed to yield a T12 model which comprises a complete 6-ring. Its formal composition is $T_{12}O_{24}$. This model was extended by substitution of two terminating hydroxyl groups with $OSi(OH)_3$ groups. Since a terminating proton substitutes a "quarter of a T atom", this means adding three TO_2 units and we obtain the T15 model with the formal composition $T_{15}O_{30}$. Subsequent ring closure of two 5-rings connected to the 6-ring resulted in the T20 model. The cluster models used by Brand et al.[26] in their investigation of the deprotonation energy of ZSM-5 at position Al12-O24-Si12 (CIS) exceed the translational period in *c* direction. Therefore, the deprotonation energies obtained from their models of increasing size approach the "dilute limit". We are interested, however, in the periodic limit of the NH_3 adsorption energies. We designed, therefore, cluster models which satisfy the criteria outlined above. Starting from the 6T model, the remaining terminating hydroxyl groups at the Brønsted acid site were first substituted by $OSi(OH)_3$ groups and the linear chain extended by a further tetrahedron to include in the QM part as much of the 10-ring as possible. The T15.5 model obtained in this way has the formal composition $T_{15.5}O_{31}$. Subsequent closure of the 6-rings around the bridging hydroxyl group yielded the T20 and T22.5 models. Figures 6 and 7 show the cluster models of the REG and CIS positions, respectively. We adopt the nomenclature "T*m*//6T", e.g. "T12/6T", which means "cluster models of formal composition $T_{12}O_{24}$ at the structure obtained by combined QM-Pot structure optimizations which use the embedded 6T models as quantum part". The T35.5 models comprise 129−134 atoms or 2143−2182 basis functions for the T(O,N)DZP basis set used, which is, even in the case of a single-point calculation only, computationally not routine. Single-point shell model potential and HF calculations were made on these models without relaxing the structure.

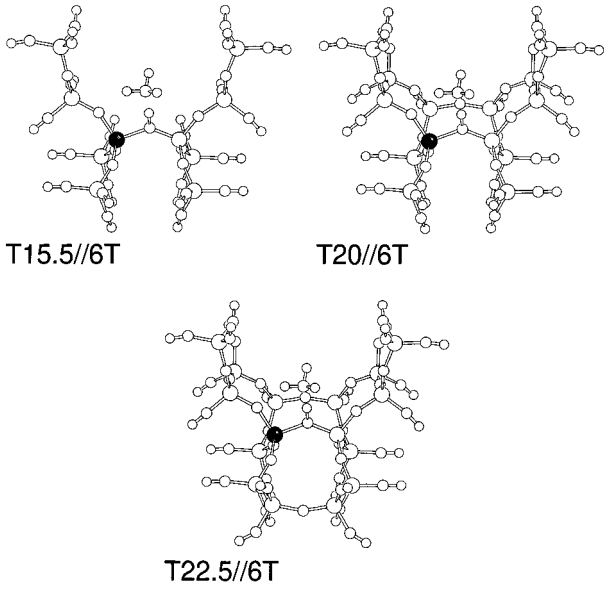

Figure 7. Clusters of increasing size embedded in NH_3·H−ZSM-5, CIS position (Al12−O24−Si12). Similar models were embedded in NH_4^+·ZSM-5^-, H−ZSM-5 and its deprotonated form.

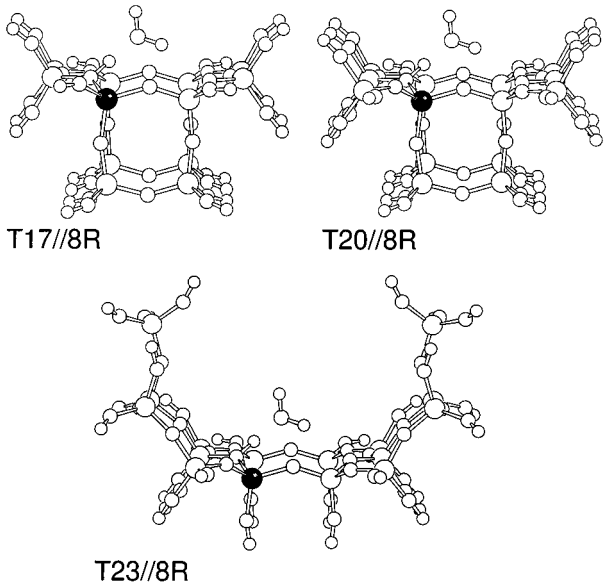

Figure 8. Clusters of increasing size embedded in NH_3·H-MOR, position Al4−O2−Si. One proton of the ammonia molecule is hidden behind the nitrogen atom. Similar models were embedded in NH_4^+·MOR^-, H-MOR and its deprotonated form.

MOR. Given the conditions discussed above, the small unit cell of mordenite does not allow much freedom in the extension of cluster models. The 8-ring model embedded at the Al4-O2-Si structure of MOR was first extended into the direction of the 8-ring pore by substitution of four terminating hydroxyl groups with silicate tetrahedra. This yields model T17. In a next step, the remaining two terminating hydroxyl groups at the Brønsted acid site were replaced by $OSi(OH)_3$ groups, resulting in model T20. Since the adsorbate is located slightly above the side pocket in the main channel, an additional way of extending the 8-ring model was considered. A T23 model was built by extending the 8-ring model with two 5−1 secondary building units.[49] To avoid overlap of cluster atoms with their periodic images, the lower tetrahedra of the side pocket in models T17 and T20 could not be considered. Figure 8 shows the cluster models used.

Table 1. Selected Bond Lengths (pm) and Angles (deg) of 6-Tetrahedra Models Embedded in the ZSM-5 Structures

	H-ZSM-5	NH_3·H−ZSM-5	NH_4^+·ZSM-5$^-$	ZSM-5$^-$
		REG (Al7−O17−Si4)		
O17−H_b	95.5	100.8		
Al7−O17	191.1	187.4	178.9	174.1
Si4−O17	169.7	167.2	160.8	157.0
H_b−N		167.0		
H_n−O17			161.0	
H_n−O17′[a]		272.5	263.1[b]	
∠Al7O17Si4	133	130	133	149
		CIS (Al12−O24−Si12)		
O24−H_b	95.7	102.4		
Al12−O24	188.4	185.0	174.3	172.5
Al12−O20	171.2	171.3	178.0	172.9
Si12−O24	168.5	165.8	158.5	156.2
H_b−N		160.8		
H_n−O24			225.2	
H_n−O20		282.3	160.2	
∠Al12O24Si12	137	135	143	150
∠Al12O20Si3	141	147	131	156

[a] At opposite side of the channel; see Figure 3. Although the space group symmetry is actually *P*1, the crystallographic position numbers of the orthorhombic framework were retained. [b] Bifurcated to O23.

6. Results and Discussion

6.1 Structures. MFI. Figures 3 and 4 show the structures of the neutral and ion-pair adsorption complexes at the REG and CIS sites of MFI. Table 1 gives the structural data obtained for the embedded 6T models by the combined QM-Pot scheme. At the REG position, the NH_4^+ ion is coordinated to four lattice oxygen atoms. If forms a short hydrogen bond to O17 and a longer bifurcated bond to O17′ and O23. Its third proton forms a long H-bond of 271 pm to O26. At the CIS position, the NH_4^+ ion is 2-fold coordinated to O20 and O24. The shorter hydrogen bond is formed with O20, which indicates that deammoniation of such a structure does probably not leave the proton at O24. This is confirmed by the energies of deprotonation, which were obtained by embedding di-tetrahedra models at the Al12-O24(H)-Si12 (1274.8 kJ/mol[8]) and the Al12-O20(H)-Si3 (1284.4 kJ/mol) sites. The larger proton affinity of O20 compared to that of O24 is another indication that Brand et al.[26] based their choice on easy accessibility of the site and not on stability.

In the neutral complexes, ammonia accepts a nonlinear Hb···-NH_3 bond and donates a N-H···O hydrogen bond to the same oxygen atom which is also involved in the hydrogen bonds formed by NH_4^+.

The structures obtained for the adsorbate-free H-ZSM-5 compare well with structures obtained by embedding smaller di-tetrahedra and 5-ring models and a larger eight-tetrahedra model.[8] The bond lengths given in Table 1 agree with those within 1 pm and the Al-O_b-Si angles within 1.5°.

MOR. Figure 5 shows the adsorbate complexes obtained by the combined QM-Pot method, and Table 2 presents selected bond lengths and angles. In the ammonium form, the NH_4^+ ion lies slightly above the side pocket in the main channel and forms two hydrogen bonds to O2 and O2′. As for NH_4^+ in the chabazite 8-ring,[38] the longer of the two hydrogen bonds does not point to an oxygen atom bound to Al, but to the neighboring silicon-bound oxygen atom. The lengths of the hydrogen bonds, 164 and 205 pm, are similar to the coordination distances in CHA (165 and 222 pm, respectively). The 2-fold coordinated NH_3 molecule adsorbed to O2-H directs one of its protons to the same oxygen atom involved in the coordination of the NH_4^+ ion. Ammonia adsorbed to O10-H did not form additional hydrogen bonds, since the acidic proton points out perpendicular to the 8-ring pore plane, resulting in the NH_3 protons being too distant from neighboring O atoms.

Table 2. Selected Bond Lengths (pm) and Angles (deg) of 8-Ring Models Embedded in the MOR Framework (Al at T4)

	H-MOR		NH_3·H-MOR			
	O2	O10	O2	O10	NH_4^+·MOR$^-$	MOR$^-$
O−H_b	95.6	95.7	102.5	101.8		
Al−O2	189.4	170.6	185.4	171.4	177.4	172.9
Al−O10	170.4	188.8	170.9	185.2	173.0	172.4
Si−O2	168.7	158.7	166.0	158.3	160.1	156.5
Si−O10	158.7	165.1	158.1	166.4	157.5	156.3
H_b−N			160.3	162.7		
H_n−O2				341.2	164.1	
H_n−O2′[a]			253.8		205.0	
∠AlO2Si	135	140	133	142	135	148
∠AlO10Si	144	136	146	136	147	151
8-ring ellipticity[b]	49.8	49.4	50.8	51.0	51.4	51.2

[a] At opposite side of the 8-ring side pocket; see Figure 5. Although the space group symmetry is actually *P*1, the crystallographic position numbers of the orthorhombic framework were retained. [b] Defined as half-difference between the longest and shortest diagonal between oxygen atoms of the 8-ring (pm).

Induced Distortions. An important feature of the combined QM-Pot scheme is that it includes the complete structural relaxation of the zeolite framework and the adsorption complex. Structure changes upon adsorption are therefore taken into account. For the following structure comparison we refer to Table 1 and Table 2. The structure changes of the neutral framework upon adsorption of the neutral molecule are small. For both ZSM-5 and MOR, stretching of the O_b−H_b bond length between 5.3 and 6.9 pm and concomitant shortening of the Al-O_b bond between 3.6 and 4 pm are observed. The changes in the Al-O_b-Si angles are between −3° and +6°. Upon proton transfer to the adsorbed NH_3, the Al-O bond lengths at the former bridging oxygen decrease between 8.0 and 10.7 pm, and the corresponding Si-O bond lengths between 5.9 and 7.4 pm. With respect to the anion, the binding of the NH_4^+ ion causes an increase of the Al-O bond length and a strong accompanying decrease of the corresponding Al-O-Si angle between 13° and 25°. The increase of the Al-O bond length is stronger where the shorter hydrogen bond is formed.

In the MOR structure one can assess the distortion of the framework induced by sorption of a molecule through the ellipticity of the 8-rings, defined as half of the difference between the longest and the corresponding perpendicular shortest diagonal between two oxygen atoms of the 8-ring. The results (Table 2) reveal that the shape of the side pocket pore remains nearly the same for all structures investigated. In both diagonals, maximum changes of 10 pm occur. The 8-ring side pocket in MOR can therefore be considered relatively nonflexible. The 8-ring is most contracted in the ion-pair structure and most expanded in the anion structure. This distortion is essentially accomplished by larger changes of the bond lengths and angles around the active site and smaller changes of the Si-O-Si angles elsewhere. Larger oval distortions of 8-rings and a concomitant shrinkage of the lattice constants were observed in zeolites consisting of double-8-ring secondary building units, e.g., zeolite rho[55,56] or merlinoite.[56]

6.2 Reaction Energies and Relative Stabilities. The energies for the reactions of the thermodynamic cycle (Scheme 1) for ammonia adsorption on the REG and CIS sites of ZSM-5

(55) McCusker, L. B. *Zeolites* **1984**, *4*, 51.
(56) Bieniok, A.; Bürgi, H.-B. In *Zeolites and Related Microporous Materials: State of the Art 1994*; Weitkamp, J., Karge, H. G., Pfeifer, H., Hölderich, W., Eds. *Stud. Surf. Sci. Catal.* **1994**, *84*, 567.

Table 3. ZSM-5, REG Position (Al7−O17−Si4). Energies of Reactions (kJ/mol) Defined in Scheme 1 from Different Embedded Cluster Models. Convergence with Increasing Cluster Size

cluster model		6T[a]	T12//6T[b]	T15//6T[b]	T20//6T[b]	T35.5//6T[b]
no. of tetrahedra		6	8	10	14	28
formal composition[c]		$T_{9.5}O_{19}$	$T_{12}O_{24}$	$T_{15}O_{30}$	$T_{20}O_{40}$	$T_{35.5}O_{71}$
adsorption	QM	−74.1	−74.2	−81.9	−83.2	−86.0
	lr[d]	−31.9	−30.2	−22.7	−19.1	−17.2
	QM-Pot	−106.0	−104.4	−104.6	−102.3	−103.2
deprotonation	QM	1350.4	1352.0	1355.5	1358.3	1326.2
	lr	−69.0	−70.5	−69.5	−75.5	−44.5
	QM-Pot	1281.4	1281.5	1286.0	1282.8	1281.7
proton transfer	QM	−15.6	−13.2	−12.3	−9.2	−16.6
	lr	−13.2	−14.2	−14.9	−12.8	−8.5
	QM-Pot	−28.8	−27.4	−27.2	−22.0	−25.1
adsorption(NC)	QM	−58.5	−61.0	−69.6	−74.0	−69.4
	lr	−18.7	−16.0	−7.7	−6.2	−8.7
	QM-Pot	−77.2	−77.0	−77.3	−80.2	−78.1
binding (IP)	QM	−518.1	−519.7	−531.0	−535.1	−505.7
	lr	+38.6	+42.0	+48.5	+58.0	+29.0
	QM-Pot	−479.5	−477.7	−482.5	−477.1	−476.7

[a] QM-Pot optimized structure. [b] "Single-point" QM-Pot calculations. [c] See text. [d] Long-range, defined in eqs 9−11.

Table 4. ZSM-5, CIS Position (Al12−O24−Si12). Reaction Energies (kJ/mol) Defined in Scheme 1 from Different Embedded Cluster Models. Convergence with Increasing Cluster Size

cluster model		6T[a]	T15.5//6T[b]	T20//6T[b]	T22.5//6T[b]
no. of tetrahedra		6	10	14	16
formal composition[c]		$T_{9.5}O_{19}$	$T_{15.5}O_{31}$	$T_{20}O_{40}$	$T_{22.5}O_{45}$
adsorption	QM	−63.1	−67.8	−73.7	−72.9
	lr[d]	−49.8	−43.5	−37.8	−38.0
	QM-Pot	−112.9	−111.3	−111.5	−110.9
deprotonation	QM	1355.5	1348.0	1350.4	1350.0
	lr	−80.1	−71.4	−74.9	−75.5
	QM-Pot	1275.4	1276.6	1275.5	1274.5
proton transfer	QM	−4.3	1.4	−4.5	−3.7
	lr	−32.0	−36.7	−30.6	−31.3
	QM-Pot	−36.3	−35.3	−35.1	−35.0
adsorption (NC)	QM	−58.8	−69.2	−69.3	−69.2
	lr	−17.8	−6.8	−7.2	−6.7
	QM-Pot	−76.6	−76.0	−76.5	−75.9
binding (IP)	QM	−512.2	−509.4	−517.7	−512.8
	lr	+32.3	+29.8	+39.0	+39.4
	QM-Pot	−479.9	−479.6	−478.7	−477.1

[a] QM-Pot optimized structure. [b] "Single-point" QM-Pot calculation. [c] See text. [d] Long-range, defined in eqs 9−11.

Table 5. MOR, Position Al4−O2−Si. Reaction Energies (kJ/mol) Defined in Scheme 1 from Different Embedded Cluster Models. Convergence with Increasing Cluster Size

cluster model		8-ring[a]	T17//8R[b]	T20//8R[b]	T23//8R[b]
no. of tetrahedra		8	12	14	16
formal composition[c]		$T_{12}O_{24}$	$T_{17}O_{34}$	$T_{20}O_{40}$	$T_{23}O_{46}$
adsorption	QM	−71.8	−80.5	−85.7	−87.7
	lr[d]	−43.9	−33.4	−27.0	−27.6
	QM-Pot	−115.8	−113.9	−112.7	−115.3
deprotonation	QM	1381.8	1355.7	1356.0	1371.1
	lr	−105.7	−78.2	−74.6	−97.6
	QM-Pot	1276.1	1277.5	1281.4	1273.5
proton transfer	QM	−8.1	−15.6	−17.1	−16.0
	lr	−25.7	−17.2	−14.9	−18.0
	QM-Pot	−33.8	−32.8	−32.0	−34.0
adsorption (NC)	QM	−63.7	−65.0	−68.6	−71.7
	lr	−18.3	−16.3	−12.1	−9.7
	QM-Pot	−82.0	−81.3	−80.7	−81.4
binding (IP)	QM	−547.2	−529.8	−535.3	−552.4
	lr	63.7	46.8	+49.6	+73.1
	QM-Pot	−483.5	−483.0	−485.7	−479.3

[a] QM-Pot optimized structure. [b] "Single-point" QM-Pot calculation. [c] See text. [d] Long-range, defined in eqs 9−11.

and on mordenite are given in Tables 3−5. The total QM-Pot energies are analyzed in terms of the QM part alone and the electrostatic long-range contributions (eq 12). We refer to the first column of each table first, which shows the results for the 6T and 8R models embedded in the ZSM-5 and MOR frameworks, respectively. For these zeolites some observations made for the FAU[37] and CHA[38] frameworks are also true. The negative binding energies for the neutral complexes (NC) and the negative adsorption energies indicate that both the neutral complex Z-OH·NH3 and the ion pair $ZO^-\cdot NH_4^+$ are stable structures. The binding energies for the neutral complexes (ZSM-5, −59 kJ/mol; MOR, −64 kJ/mol) have about the same

Table 6. Relative Stabilities (kJ/mol) of the CIS Position in ZSM-5 with Respect to the REG Position, and of the O10 Position in MOR with Respect to O2, Obtained from the QM-Pot Energies of Embedded 6T (ZSM-5) and 8R (MOR) Models

zeolite	position	Z-OH	Z-OH·NH_3	ZO^-·NH_4^+	ZO^-
ZSM-5	REG → CIS	12.8	13.4	5.9	6.6
MOR	O2 → O10		10.3	15.7	

magnitude as the energies of NH_3 adsorption obtained by ab initio calculations on various gas-phase models (cf. Table 17 of ref 16). For all sites, the QM energies of formation of the ion pair from the neutral components (adsorption energies) are larger than the adsorption energies of the NC.

We compare now the NH_3 adsorption on different oxygen positions for the same zeolite. For ZSM-5 different Al-O-Si sites are compared. The deprotonation energies for the REG (1281 kJ/mol) and the CIS (1275 kJ/mol) positions reveal that the REG site is the less acidic and therefore preferred to proton occupation. The relative stabilities (Table 6) calculated from the total QM-Pot energies of the two positions support this. For all forms, with or without adsorbate, the CIS position is less stable by at least 5.9 kJ/mol. The free Brønsted site and the neutral complex are destabilized by 12.8 and 13.4 kJ/mol, respectively.

Comparison of the deprotonation energies obtained by embedding 6T models with earlier values obtained on smaller embedded di-tetrahedra models[8] shows that the mechanical embedding scheme is quite stable with respect to relaxation of embedded cluster models of different size. For both positions, the difference between the smaller and the larger model is less than 5 kJ/mol.

Both the REG and the CIS positions exhibit very similar binding energies for the neutral complex (−77 kJ/mol) and the ion pair (−478 to −479 kJ/mol). The energy of NH_4^+ formation from ammonia and the neutral zeolite (adsorption energy) is slightly higher by 7 kJ/mol for the CIS site (−113 kJ/mol) than that for the REG site.

For mordenite, two oxygen positions which belong to the same AlO_4^- tetrahedron are compared. The QM-Pot deprotonation energy at position O2-H (1276 kJ/mol) is higher by 15 kJ/mol with respect to O10-H (1261 kJ/mol). Protonation of the O2 site is therefore highly preferred, and the acidity of the O2-H group is smaller. Binding of NH_3 on the acidic proton at position O2-H is weaker by 5 kJ/mol with respect to O10-H. This adsorption position is not favored, since its QM-Pot energy is higher by 10.8 kJ/mol than that of NH_3 adsorbed on the O2-H site. That proton location at O2-H is preferred is also supported by the QM-Pot energy of proton transfer to ammonia adsorbed to this position, which is lower by 10 kJ/mol compared to proton transfer from O10-H.

Selection of Basis Set. From experiment it is clear that the interaction of NH_3 with Brønsted acid sites is so strong that NH_4^+ ions are formed.[10−13] The mechanical embedding calculations confirm this for all sites investigated, since the absolute value of the QM energy of NH_4^+ ion formation from the zeolite proton and ammonia is larger than the binding energy of the NC. That the ammonium ion adsorbed in zeolites is more stable than ammonia is also reflected by the negative QM proton-transfer energies in Table 3−5. Ab initio calculations and other embedding schemes which apply smaller basis sets[57] often fail to describe the ion pair as more stable than the neutral complex.[16] The reason for this is that nonflexible basis sets, e.g., STO−3G, are not appropriate for describing the anion in the ion pair. In cluster calculations the ion-pair structure was found more stable provided that reasonable basis sets (double-ζ plus polarization) were applied and proper models were used,[16] which allow the ammonium ion to form hydrogen bonds with two or three oxygen atoms bound to aluminum.[16,22−25] These conditions are easily fulfilled by using the present embedding scheme.

6.3. Stability of the QM-Pot Results with Increasing Cluster Size. The stability of the QM-Pot results with increasing cluster size provides strong support for the soundness of our method. The ab initio studies of Brand et al. on cluster models containing up to 46 T atoms (T = Si, Al) cut out from ZSM-5 showed that the calculated deprotonation energies depend on the shape of the cluster and are slowly convergent with increasing cluster size.[26,27] Their calculation of the electrostatic potential in the region of the bridging hydroxyl group indicated that this dependence is primarily due to electrostatic effects. Our embedding scheme includes such effects, as the long-range electrostatic and polarization contributions are calculated by the shell model potential. Depending on the size of the embedded cluster, this contribution to the total QM-Pot reaction energy is considerable, e.g., −43.9 kJ/mol (38%) for adsorption of ammonia at the O2-H site in mordenite (Table 5). Based on previous results for faujasite,[37] we expect this potential term to decline and the quantum mechanical part to grow with increasing size of the embedded cluster. Therefore, we used clusters of increasing size to check the convergence behavior for ZSM-5 and mordenite.

Table 3 and Table 4 contain the results for the REG and CIS positions, respectively. Although the electrostatic long-range contributions converge slowly, the total QM-Pot energies are remarkably stable with increasing cluster size. For the adsorption energies of NH_3 and NH_4^+ from the neutral molecule and the bridging hydroxyl group at the REG position, the long-range part decreases by about 15 and 10 kJ/mol, respectively, while the total QM-Pot result stays the same within 4 kJ/mol. We find a similar stability of the QM-Pot energies for the CIS position.

We note, however, that for the deprotonation energy and the ion-pair binding energy of the REG position the absolute value of the long-range part does not decrease as expected, but increases slightly up to a cluster size of $T_{20}O_{40}$. The total QM-Pot energies, however, remain stable since the QM energies show the opposite trend ("reverse" convergence). In both reactions the anion is involved. In all models up to $T_{20}O_{40}$, the silicon atom of the Al-O(H)-Si bridge is saturated with a terminal hydroxyl group only, which might be the reason for the reverse convergence observed in this case. A larger model in which these groups are fully substituted by silicate tetrahedra is model T35.5 shown in Figure 6. When increasing the cluster size from T20 to T35.5, we find a large drop of the QM part of the deprotonation energy from 1358 to 1326 kJ/mol and a corresponding increase of the lr part from −76 to −45 kJ/mol. A similar large drop is found for the lr part of the binding energy of the IP. Hence, the "reverse" convergence behavior of the individual QM and lr parts exhibited by the smaller models is remedied. Most important, both parts add up to total QM-Pot reaction energies which are within or close to the range covered by the smaller models. For all reactions the QM-Pot energies are stable within 7 kJ/mol. The total QM-Pot reaction energies for mordenite presented in Table 5 show the same stability. Our results support the observation already made by Brand et al. that QM energies vary considerably with size and shape of the

(57) Pisani, C.; Birkenheuer, U. *Int. J. Quant. Chem.: Quant. Chem. Symp.* **1995**, *29*, 221.

Table 7. Energies of NH_4^+ Formation from Neutral Zeolites and NH_3 Including Electron Correlation (kJ/mol). Basis Set: T(O,N)DZP

	FAU, O1	CHA, O1		MOR, O2		ZSM-5, REG	
ΔE	3T//3T[a]	8R[b]	4T//8R	8R	4T//8R	6T	4T//6T
QM-Pot	−109	−109		−116		−106	
SCF//QM-POT	−54		−45		−52		−34
ΔMP2	−33		−35		−34		−32
CPC	+15		+16		+17		+15
total[c]	−127	−128		−133		−123	
ref	37, 59	38		this work		this work	

[a] "3T//3T" notation denotes "three-tetrahedra model at structure of embedded 3-tetrahedra model". [b] "8R" notation denotes 8-membered ring. [c] Total = QM-Pot + ΔMP2 + CPC.

cluster model.[26,27] Comparison of reaction energies obtained on gas phase clusters of different size designed to model different active sites of a zeolite framework as was done in a recent MNDO study[58] is therefore of limited predictive value. It is mandatory to include the long range influence of the zeolite framework, which is easily achieved within our embedding scheme. Since an essential part of the reaction energy is electrostatic interaction of the active site with surrounding atoms, relatively small embedded clusters may already yield converged QM-Pot reaction energies provided that electrostatics are included. An important requirement is, however, that short range interactions driving the structural relaxation of the active site and the adsorbate are included in the QM part of the embedding scheme. After having shown that the embedded cluster results are stable within a few kJ/mol we will use in the following discussions the QM-Pot energies obtained from the structure optimizations in the first column of Tables 3 and 5.

6.4. Estimate of Electron Correlation Contributions. Since all calculations mentioned so far are made at the Hartree-Fock level, electron correlation effects are added a posteriori by single-point MP2 calculations. MP2 calculations with a T(O,N)DZP basis set on 8-ring or 6-tetrahedra models are computationally very demanding. Therefore, smaller 4-tetrahedra (4T) clusters which include the main hydrogen bond interactions of NH_3 and NH_4^+ with the zeolite framework were cut out from the structures obtained by embedding the larger models. The essential short-range correlation effects such as dispersion are included this way, but long-range effects via changes of the charge distribution are neglected. Table 7 lists the results and compares them with energies of NH_3 adsorption on the most stable proton positions of faujasite[37,59] and chabazite.[38] In the case of faujasite, a tri-tetrahedra model was used for both the embedding and the single-point MP2 calculations. For all four zeolite frameworks investigated (ZSM-5, MOR, FAU, CHA), electron correlation increases the energy of NH_3 adsorption by about 32−35 kJ/mol (in absolute terms). However, about half of the effect is due to the basis set superposition error (BSSE) which reduces the adsorption energy by 15−17 kJ/mol (in absolute terms). The BSSE was calculated with the full counterpoise correction (CPC) according to Boys and Bernardi.[60] We find that the BSSE corrected contributions of the electron correlation show only small variations within a range of 2 kJ/mol over the four different zeolites. We conclude that electron correlation changes the absolute value of the heat of NH_3 adsorption, but does not affect the sequence obtained from the combined QM-Pot calculations at the Hartree-Fock level (Table 8). Because the limited size of our basis set, we expect our estimates of electron correlation effects to be lower limits (in absolute terms).

Embedded cluster calculations on ammonia sorption on H-faujasite were also carried out by Greatbanks et al.[42] Hydrogen terminated tri-tetrahedra clusters were embedded into a lattice of point charges. The MP2 calculations used a 6-31G** basis set. Relaxation was allowed only for the AlO_4(H) core and the adsorbate. The adsorption energy (formation of NH_4^+ from the neutral components) of −145 kJ/mol (not corrected for the BSSE) is of similar size as our not corrected result which is −127 − 15 = −142 kJ/mol (cf. Table 7). As in our calculations, the formation of NH_4^+ is favored over the formation of a neutral adsorption complex.

6.5. Comparison between Zeolite Frameworks. The main potential of the present QM-Pot embedding scheme is its ability to discriminate between catalytically active sites in different crystallographic positions of a framework and between different zeolite frameworks. Table 8 summarizes our QM-Pot results for the most stable Brønsted acid sites in ZSM-5 and mordenite and includes also results of the high-silica modifications of zeolites faujasite[37,59] and chabazite.[38] Although the Si/Al ratios are not identical, the compositions investigated already represent good models for isolated Brønsted sites. This was confirmed by shell model calculations of the deprotonation energy of the chabazite structure, which has the smallest unit cell volume and the Si/Al ratio of 11 which is the smallest of the four zeolites. Its deprotonation energy is therefore expected to show the largest changes upon decrease of the Al content. Upon increase of the Si/Al from 11 to 23, the deprotonation energy is lowered by 6.6 kJ/mol. The deprotonation energy of H-faujasite changes by 2 kJ/mol only when going from Si/Al = 47 to Si/Al = 95. In Table 8, the zeolites are ordered according to increasing deprotonation energy.

The structural data of the bridging hydroxyl groups provided in Table 8 might suggest a correlation between the change of the Al-O-Si angle upon deprotonation and the deprotonation energy. However, inclusion of additional data of various Brønsted acid sites, e.g., for faujasite[8] and for the weaker sites in mordenite and ZSM-5 shows that such a simple relation does not hold.

According to the calculated deprotonation energies, high-silica faujasite hosts the most acidic Brønsted sites while ZSM-5 has the least acidic. This relation has been discussed before[8] and two remarks should be made. The difference is neither explained by local structure effects nor by crystal potential effects alone. This is supported by the decomposition of ΔE_{DP} obtained from embedded di-tetrahedra models (Table 8). The observation that H-Y zeolites are less acidic than H-ZSM-5 catalysts is due to the high Al content in the faujasite framework of HY. The calculated values for chabazite and mordenite fall into the range between the two extremes.

The energies of adsorption (formation of NH_4^+) do not indicate the same acidity sequence as the energies of deprotonation. The former differ from the latter by the ion-pair binding energy (Scheme 1). This ion-pair binding energy, ΔE_{IP}, is not constant, as Table 8 shows. There are two types of effects. The first one is the general trend that the ion-pair binding becomes stronger when the acidity becomes weaker. This is easily explained by the properties of conjugated acid−base pairs. The anion ZO^- formed by deprotonation of the weaker acid Z−OH is a stronger base. The stronger base forms stronger

(58) Redondo, A.; Hay, P. J. *J. Phys. Chem.* **1993**, *97*, 11754.

(59) Closer inspection of the NH_4-faujasite structure obtained with an embedded tri-tetrahedra model revealed that the structure found was lying on a saddle-point of the PES. The QM-Pot energy of the converged structure is by 3 kJ/mol lower. We report here the corresponding correct results.

(60) Boys, S. F.; Bernardi, F. *Mol. Phys.* **1970**, *19*, 553.

Table 8. Comparison of Zeolite Acidities between Different Frameworks and Relation to Structural Data of the Bronsted Acid Site and the Adsorbed NH_4^+ Ion. Results from QM-Pot[a] Calculations. Energies (kJ/mol), Bond Lengths (pm), and Angles (deg) Are Presented

framework	FAU	CHA[b]	MOR	MFI
site	O1 (O4)	O1 (O3′)	(O2′)	Al7−O17−Si4 (REG)
cavity	supercage	8-ring	main/side	sinusoidal
pore size	710 × 755	326 × 437	378 × 480	509 × 590
Si/Al	47	11	47	95
embedded model	3T	8R	8R	6T
$r(O_b-H_b)$	95.5	95.8	95.7	95.5
$r(Al-O_b)$	190.4	191.3	191.1	189.4
$r(Si-O_b)$	170.1	170.4	169.7	168.7
∠SiO(H)Al	127	136	135	133
∠SiO⁻Al (anion)	138	148	149	149
Δ∠SiOAl	11	12	14	16
		Z-H → Z^- + H^+		
ΔE_{DP}^{QM-Pot}	1252	1271	1276	1281
ΔE_{DP}^{QM-Pot} (2T)[c]	1250[d]	1277	1281	1286[d]
long-range (2T)[c]	−119[d]	−76	−107	−77[d]
QM (2T)[c]	1369[d]	1353	1388	1363[d]
		Z^- + NH_4^+ → NH_4^+·Z^-		
ΔE_{IP}^{QM-Pot}	−457	−476	−484	−480
		Z-H + NH_3 → NH_4^+·Z^-		
ΔE_{Ads}^{QM-Pot}	−109	−109	−116	−106
$r(H_N$-O)	153	165	164	161
	229	222	205	263
		Z-H + NH_3 → Z-H·NH_3		
$\Delta E_{Ads(NC)}^{QM-Pot}$	−81	−75	−82	−77

[a] QM, SCF/T(O,N)DZP; Pot, shell model potential. [b] Results based on an averaged structure for a periodic calculation. The averaging introduces deviations of 2−7 kJ/mol.[38] Numbering of atoms according to ref 78. [c] Decomposition of deprotonation energy for embedded di-tetrahedra (2T) models. [d] Reference 8.

H-bonds with the "acid" NH_4^+ in the ion pair ZO^-·NH_4^+. This explains the results within the series FAU, CHA, MFI with the exception of MOR. The second type has more subtle effects of the interaction of NH_4^+ with the negatively charged zeolite surface. An example is MOR which has a higher acidity than MFI but its conjugated base also binds NH_4^+ more strongly than the conjugated base of MFI. Neither the binding energies for the ion pairs nor for the neutral complexes listed in Table 8 do show any dependence on the pore size as discussed by Derouane et al.[61] for physisorbed molecules. In the large pore faujasite framework, NH_4^+ forms two hydrogen bonds to oxygen atoms of the same AlO_4^- tetrahedron. In the smaller 8-ring and 10-ring pores occurring in CHA, MOR (side pockets), and ZSM-5, the second hydrogen bond of NH_4^+ is not formed to an oxygen atom bound to Al, but to a next-neighbor O atom linked to two Si. Except for faujasite, where the two protons of the ammonium ion coordinate to oxygen atoms bound both to Al, we find that shortening of one hydrogen bond implies lengthening of the second hydrogen bond. A similar coordination behavior was observed for methanol adsorbed in the 8-ring of CHA.[34]

6.6. Comparison with Experiment. Heats of deprotonation of zeolites have been inferred from observed shifts of the OH stretching frequencies of bridging hydroxyls on adsorption of various molecules and comparing them with OH frequency shifts of standard OH acids of known gas-phase acidity on adsorption of the same set of base molecules (Bellamy−Hallam−Williams relation[7]). Such heats of deprotonation for H-ZSM-5 and H-faujasite were already presented and discussed.[8] For H-mordenite (Si/Al = 9−12.5), heats of deprotonation of 1185 ± 5 kJ/mol were determined.[62] For H-chabazite no experimental data are available. For comparison with experiment, the calculated energy of deprotonation (Table 8) needs corrections for the systematic error of the computational technique and finite temperature nuclear motion effects. From a previous study, the systematic deviation due to neglect of electron correlation and basis set truncation is known to be −46 kJ/mol for the T(O)-DZP basis set. ZPE and thermal corrections contribute −35 kJ/mol.[16] Our final estimate for the heat of deprotonation of high-silica H-MOR, 1276 − 46 − 35 = 1195 kJ/mol (cf. Table 5), compares well with the experimental value (1185 ± 5 kJ/mol). While there is agreement between the range of "observed" values reported for various zeolites (1142 − 1236 kJ/mol; cf. Table 18 of ref 8 and the result for MOR quoted here), the scatter of data for a given system (different base molecules, different reference acids) makes it difficult to establish an acidity scale for a series of well-defined catalysts. This is the strength of theoretical predictions, which are not affected by any assumptions. Hence, our predicted values of 1171, 1190, 1195, and 1200 kJ/mol for Brønsted sites in high-silica FAU, CHA, MOR, and MFI seem to be the most reliable estimates of relative heats of deprotonation.

The comparison of predicted heats of NH_3 adsorption for zeolites with experimental values is difficult, since the observed heats reported scatter considerably depending on the sample preparation (steaming, acid leaching, completeness of NH_4^+ exchange, calcination), catalyst composition (framework Si/Al ratio, presence of extralattice Al), and the method used (temperature-programmed desorption or microcalorimetry).[9] TPD measurements on two different samples, H-ZSM-5 with Si/Al = 25 and Si/Al = 33, yielded most frequent activation energies of desorption of 110 and 104 kJ/mol, respectively.[63] Niwa et al. obtained values of 131−133 kJ/mol for two ZSM-5 samples (Si/Al = 20 and 70) with a different deconvolution method.[64]

(61) Derouane, E. G.; André, J.-M.; Lucas, A. A. *J. Catal.* **1988**, *110*, 58.

(62) Soltanov, R. I. *Kinet. Katal.* **1990**, *31*, 438.

(63) Karge, H. G. In *Catalysis and Adsorption by Zeolites*; Öhlmann, G., Pfeifer, H., Fricke, R., Eds.; Elsevier: Amsterdam, 1991; p 133.

(64) Niwa, M.; Katada, N.; Sawa, M.; Murakami, Y. In *Zeolite Science 1994: Recent Progress and Discussions*; Karge, H. G., Weitkamp, J., Eds. *Stud. Surf. Sci. Catal.* **1995**, *98*, 101.

Table 9. Predicted and Observed Heats of NH_3 Adsorption (Negative Values, kJ/mol)

framework	MFI	FAU	CHA	MOR
calcd	109	113	114	119
Si/Al	95	47	11	47
MC	145−150[a]	115−130[b]	155[c]	160[d]
Si/Al	>27[a]	5.6[b]	4.5[c]	20−46[d]
TPD	104−110,[e] 131−133[f]	104−111[g]		115−117,[h] 146−154[f]
Si/Al	33−25,[e] 20−70[f]	2.4−5.8[g]		12−39,[h] 10−20[f]

[a] References 65−67. [b] Reference 74. [c] Reference 75. [d] References 66, 67, 70, 71. [e] Reference 63. [f] Reference 64. [g] References 72 and 73. [h] References 63 and 68.

Heats of adsorption obtained by microcalorimetry for H-ZSM-5[65,66] and Na,H-ZSM-5[67] (Si/Al > 27) are in a close range of 145−150 kJ/mol. Karge and Dondur deconvoluted the TPD spectra of NH_3 on mordenites dealuminated by acid leaching (Si/Al = 12−39), and attributed two peaks to weaker and stronger Brønsted acid sites with heats of NH_3 desorption of 100−104 kJ/mol and 115−117 kJ/mol,[63,68] respectively. Based on the comparison with TPD of pyridine, they assume that the stronger Brønsted acid sites are localized in such parts of the mordenite structure where they are easily accessible for NH_3 but not for pyridine molecules. These are probably the side pockets, as supported by adsorption−desorption studies of ammonia, benzene, and cyclohexane in combination with FTIR spectroscopy.[69] In contrast, Niwa et al. report higher TPD values of 146−154 kJ/mol for H-mordenites with Si/Al ratios between 10 and 20.[64] For mordenites having Si/Al_f > 20, several microcalorimetry studies consistently report heats of NH_3 adsorption of about 160 kJ/mol.[66,67,70,71] From Si/Al = 5.8 up to Si/Al = 16, the initial heat of adsorption decreases from 160 to 140 kJ/mol, and then increases again with increasing Si/Al ratio.[70,71] Experimental data for faujasites[72−74] were discussed in ref 37. For chabazite, only calorimetric data are available.[75]

Table 9 summarizes the TPD and microcalorimetry data. Heats of NH_3 adsorption inferred from microcalorimetry are by 10−40 kJ/mol larger than those inferred from TPD, with the exception of faujasite. However, both methods yield the largest heat of adsorption for mordenite and a difference between the heats for mordenite and ZSM-5 of 10−23 kJ/mol. The lower heat of NH_3 adsorption observed for faujasite is probably due to its lower Si/Al ratio.

Our QM-Pot scheme provides reliable estimates of heats of NH_3 adsorption on ideal zeolite structures with tunable concentration of active sites. For final comparison with experiment, the calculated values in Table 8 ("total") still need corrections for zero-point energy (ΔZPE) and thermal contributions $\Delta\Delta H$(T). From previous SCF calculations on a H-saturated pentameric cluster (shell-2), values of +16 and +14 kJ/mol are known for ΔZPE and ΔZPE + $\Delta\Delta H$(T), respectively.[16] Our final estimates listed in Table 9 lie in a close range of 109−119 kJ/mol and follow the acidity sequence MOR > CHA ≈ Y > ZSM-5. Again with the already mentioned exception of the low Si/Al faujasite, this compares well with the fact that observed heats of NH_3 adsorption are highest for mordenite and lowest for ZSM-5. The calculated values lie closer to the range of adsorption heats observed by TPD than those by microcalorimetry. This does not imply that comparison with TPD values should be preferred. TPD results are in general less reliable and severely depend on the preparation and measurement conditions.[9] Recent careful TPD measurements on nonpretreated ZSM-5 samples yield the same heat of adsorption as MC (145 kJ/mol).[76] Use of larger basis sets will probably increase the calculated heats of adsorption. Also a more complete determination of ZPE effects from the whole zeolite lattice is required. Nevertheless, the calculated consistent differences in acidity of 5 kJ/mol between MOR and CHA and between CHA and ZSM-5 are in good accordance with the observed differences. The predicted difference of 10 kJ/mol between MOR and ZSM-5 is supported by the microcalorimetric data of Gorte et al.[65,66] and Dumesic et al.[67]

Heats of deprotonation and heats of NH_3 adsorption yield different acidity sequences (Table 8): Y > CHA > MOR > ZSM-5 for deprotonation, and MOR > CHA ≈ Y > ZSM-5 for adsorption. The calculated deprotonation energies are more sensitive to the change of the framework type and show differences as large as 30 kJ/mol. In contrast, calculated energy differences for NH_3 adsorption are small and lie in a close range of 10 kJ/mol. The heat of deprotonation is an intrinsic property of the zeolite framework, while on adsorption of NH_3 there is an interaction of NH_4^+ with the surface. This may be considered as a model of the interaction of the reactant with the catalyst in a catalytic reaction. However, the interaction of hydrocarbons with the catalytically active sites may be different from that of NH_4^+ which is dominated by H-bonds.

Our study demonstrates for ammonia how the interaction of the base with the zeolite framework changes the acidity scale based on adsorption data compared to the scale based on deprotonation energies. Different base molecules may yield different acidity scales due to different interactions with the zeolite surface. Strong evidence for such behavior is provided by the microcalorimetric measurements of Gorte and coworkers.[77] For the same high-silica sample of either ZSM-5 or mordenite, they determined average differential heats of adsorption for a series of substituted amines and pyridines. They showed that depending on the choice of the base either ZSM-5 or MOR proves more acidic. Relative acid strengths based on the adsorption scale depend on the specific interactions the protonated base can undergo with the deprotonated framework.

7. Conclusions

An embedded cluster scheme which combines a QM description for the active site with an interatomic potential function for the periodic zeolite (QM-Pot) is capable of modeling the influence of various zeolite frameworks on the acidity of Brønsted sites. Calculations on embedded clusters of different shape and size show that the QM reaction energies obtained for the cluster model vary significantly and are only slowly convergent with increasing cluster size. Adding long-range

(65) Parrillo, D. J.; Gorte, R. J.; Farneth, W. E. *J. Am. Chem. Soc.* **1993**, *115*, 12441.
(66) Parrillo, D. J.; Gorte, R. J. *J. Phys. Chem.* **1993**, *97*, 8786.
(67) Chen, D. T.; Zhang, L.; Yi, C.; Dumesic, J. A. *J. Catal.* **1994**, *146*, 257.
(68) Karge, H. G.; Dondur, V. *J. Phys. Chem.* **1990**, *94*, 765.
(69) Zholobenko, V. L.; Makarova, M. A.; Dwyer, J. *J. Phys. Chem.* **1993**, *97*, 5962.
(70) Stach, H.; Jänchen, J.; Jerschkewitz, H.-G.; Lohse, U.; Parlitz, B.; Hunger, M. *J. Phys. Chem.* **1992**, *96*, 8480.
(71) Stach, H.; Jänchen, J.; Jerschkewitz, H.-G.; Lohse, U.; Parlitz, B.; Zibrowius, B.; Hunger, M. *J. Phys. Chem.* **1992**, *96*, 8473.
(72) Karge, H. G.; Dondur, V.; Weitkamp, J. *J. Phys. Chem.* **1991**, *95*, 283.
(73) Hunger, B.; v Szombathely, M. *Z. Phys. Chem.* **1995**, *190*, 19.
(74) Lohse, U.; Parlitz, B.; Patzelová, V. *J. Phys. Chem.* **1989**, *93*, 3677.
(75) Zones, S. I.; Harris, T. V.; Auroux, A., Unpublished results.
(76) Haag, W. O. Private communication.
(77) Lee, C.; Parrillo, D. J.; Gorte, R. J.; Farneth, W. E. *J. Am. Chem. Soc.* **1996**, *118*, 3262.
(78) Calligaris, M.; Nardin, G.; Randaccio, L.; Comin-Chiaramonti, P. *Acta Crystallogr., Sect. B* **1982**, *38*, 602.

corrections for the periodic zeolite structure yields total QM-Pot energies which are remarkably stable with respect to the choice of the embedded cluster.

The QM-Pot scheme is used to investigate the acid strength of the most stable Brønsted acid sites of the high-silica frameworks faujasite, chabazite, mordenite, and MFI. Both the heat of deprotonation and the heat of NH_3 adsorption are considered as measures of acid strength. The calculated deprotonation energies are more sensitive to the change of the framework type and show differences as large as 30 kJ/mol, which are neither explained by local structure effects nor by crystal potential effects alone. The calculated heats of deprotonation suggest the acidity sequence Y (1171 kJ/mol) > CHA (1190 kJ/mol) > MOR (1195 kJ/mol) > ZSM-5 (1200 kJ/mol). In contrast, the calculated heats of NH_3 adsorption suggest the sequence MOR > CHA ≈ Y > ZSM-5. The predicted heats of NH_3 adsorption are −119, −114, −113, and −109 kJ/mol, respectively, including estimates of electron correlation and nuclear motion effects. These values are assumed to be lower estimates (in absolute terms). In agreement with microcalorimetry data we predict the heat of NH_3 adsorption to be 10 kJ/mol larger for MOR than for MFI.

The different sequence for deprotonation energies and heats of adsorption is caused by specific interactions of NH_4^+ with the negatively charged catalyst surface. Low deprotonation energies (reflecting high intrinsic acidity) appear to be partially correlated with low binding energies of the ion pair. Making the zeolite a stronger acid makes the deprotonated zeolite a weaker base which forms weaker hydrogen bonds with the ammonium ion formed on NH_3 adsorption.

Acknowledgment. We thank J. D. Gale (London) and R. Ahlrichs (Karlsruhe) for providing recent versions of the GULP and TURBOMOLE codes, respectively. The SSZ-13 adsorption data were kindly provided by T. V. Harris, S. I. Zones (Chevron, Richmond), and A. Auroux (Lyon). We thank U. Eichler and K.-P. Schröder for providing shell model results on H−ZSM-5. M. B. acknowledges the Alexander-von-Humboldt Foundation for a research fellowship. This work has been supported by the "Fonds der Chemischen Industrie", the Max-Planck-Society, and by a consortium of industrial and academic members within the "Catalysis and Sorption Project" of Molecular Simulations Inc.

Supporting Information Available: Detailed lattice constants of the MFI and MOR frameworks obtained by lattice energy minimizations (1 page). See any current masthead page for ordering information and Web access instructions.

JA9729037